

This is the accepted manuscript made available via CHORUS. The article has been published as:

Investigation of discrete states and quasidiscrete structures observed in ^{150}Sm and ^{152}Sm using the (p,γ) reaction

P. Humby, A. Simon, C. W. Beausang, J. M. Allmond, J. T. Burke, R. J. Casperson, R. Chyzh, M. Dag, K. Gell, R. O. Hughes, J. Koglin, E. McCleskey, M. McCleskey, S. Ota, T. J. Ross, A. Saastamoinen, T. Tarlow, and G. Vyas

Phys. Rev. C **94**, 064314 — Published 14 December 2016

DOI: [10.1103/PhysRevC.94.064314](https://doi.org/10.1103/PhysRevC.94.064314)

Investigation of discrete states and quasi-discrete structures observed in ^{150}Sm and ^{152}Sm using the (p,t- γ) reaction

P. Humby,^{1,2} A. Simon,^{1,3} C. W. Beausang,¹ J. M. Allmond,⁴ J. T. Burke,⁵ R. J. Casperson,⁵ R. Chyzh,⁶ M. Dag,⁶ K. Gell,¹ R. O. Hughes,⁵ J. Koglin,⁵ E. McCleskey,⁶ M. McCleskey,⁶ S. Ota,⁵ T. J. Ross,⁷ A. Saastamoinen,⁶ T. Tarlow,¹ and G. Vyas¹

¹*Department of Physics, University of Richmond, Richmond, Virginia 23171, USA*

²*Department of Physics, University of Surrey, Surrey, GU27XH, UK*

³*Department of Physics, University of Notre Dame, Notre Dame, IN 46556*

⁴*Physics Division, Oak Ridge National Laboratory, Oak Ridge, Tennessee 37831, USA*

⁵*Lawrence Livermore National Laboratory, Livermore, California 94551, USA*

⁶*Cyclotron Institute, Texas A&M University, College Station, Texas 77843, USA*

⁷*Department of Chemistry, University of Kentucky, Lexington, Kentucky 40506, USA*

New levels and γ -ray transitions were identified in $^{150,152}\text{Sm}$ utilizing the (p,t) reaction and particle- γ coincidence data. A large, peak-like structure observed between 2.3-3.0 MeV in excitation energy in the triton energy spectra was also investigated. The orbital angular momentum transfer was probed by comparing the experimental angular distributions of the outgoing tritons to calculated DWBA curves. The angular distributions of the outgoing tritons populating the peak-like structure are remarkably similar in the two reactions, and are significantly different to the angular distributions associated with the nearby continuum region. Relative partial cross sections for the observed levels, angle averaged between 34 and 58 degrees, were measured. In ^{150}Sm 39(4)% of the strength of the peak-like structure could be accounted for by the observed discrete states. This compares to a value of 93(15)% for ^{152}Sm .

I. INTRODUCTION

The samarium ($Z=62$) isotopes near $N=90$ lie in a region of rapid shape change from spherical to deformed with increasing neutron number. This has led to this region of the nuclear chart being the focus of intense experimental and theoretical study, see for example references [1–6]. In the early two-neutron transfer experiments by Maxwell [7] and Bjerregaard [8] excited $J^\pi = 0^+$ states were observed to have large cross sections relative to the ground state in the $^{152}\text{Sm}(p,t)$ and $^{150}\text{Sm}(t,p)$ reactions. This was interpreted in terms of shape coexistence [7, 8] and the rapid onset of deformation, inviting further interest in these nuclei. In general, the $N=90$ region provides a rich testing ground for models that attempt to describe transitional and deformed nuclei.

Two-neutron transfer reactions provide an excellent tool with which to study both the removal of pairs of correlated neutrons from valence orbitals, typically populating states at relatively low excitation energies, as well as the removal of neutrons from deep below the Fermi surface. Following the work of Maxwell [7], further $\text{Sm}(p,t)$ experiments were performed with improved energy resolution for the outgoing tritons, see for example [9–12], at various incident proton beam energies. In the 1981 study by Struble *et al.* [13] a large, broad enhancement of two-neutron transfer strength at an excitation energy of approximately 6 MeV was observed in the $^{148,150,152,154}\text{Sm}(p,t)$ reactions. An additional, much narrower, peak-like structure at an excitation energy of 2.2-3.1 MeV was observed in both the $^{152,154}\text{Sm}(p,t)$ reactions. In the $^{158}\text{Gd}(p,t)^{156}\text{Gd}$ study by Riezebos *et al.* [14] a rapid increase in 2^+ , 4^+ and 6^+ strength was ob-

served above 2 MeV in excitation energy. An interesting lack of monopole strength was reported above this energy, providing motivation to study the L-transfer distribution at this excitation energy in nearby nuclei.

In the present work, the peak-like structure (PLS) is studied in detail and $^{150,152}\text{Sm}$ are studied for the first time using the (p,t- γ) coincidence technique. The coincident detection of the γ ray allows for excellent selectivity and sensitivity and allows us to identify multiple new levels and γ -ray transitions in each nucleus. Triton angular distributions, selected by specific γ -ray transitions, probe the angular momentum transfer to both low lying discrete states and states in the PLS, and are compared to calculated DWBA curves.

II. EXPERIMENTAL ARRANGEMENT

A 25 MeV proton beam from the K-150 cyclotron at the Cyclotron Institute of Texas A&M University was incident upon isotopically enriched ^{152}Sm and ^{154}Sm targets of 98% and 99% purity respectively and approximately 1 mg cm^{-2} thickness. The ^{152}Sm target was bombarded for 42 h and the ^{154}Sm target for 35 h with average beam currents of 1.4 nA and 1.2 nA, respectively.

The outgoing light ions and γ rays were detected using the STARLiTeR array, which uses the same configuration as that described in detail in reference [15]. This array consisted of the STARS (Silicon Telescope Array for Reaction Studies) ΔE - E silicon telescope and the LiTeR (Livermore Texas Richmond) array of BGO shielded HPGe clover detectors providing particle- γ and particle- γ - γ coincidence capability. A total of 1.5×10^5 t- γ - γ coincidences were observed for the $^{152}\text{Sm}(p,t)$ reac-

tion and 1.4×10^5 for the $^{154}\text{Sm}(p,t)$ reaction, allowing $t\text{-}\gamma\text{-}\gamma$ measurements for only the strongest transitions. STARS consisted of a 0.14 mm thick ΔE detector and a 1 mm thick E detector, both segmented into 24 rings (θ) and 8 sectors (ϕ). The distance between the target foil and the ΔE detector was 18 mm. The angular coverage of the telescope was 34 to 58 degrees. An aluminum δ -shield was placed between the target position and STARS in order to shield the ΔE detector from secondary electrons. An aluminum tunnel passed through the center of the telescope in order to shield the inner rings from scattered beam particles. The six HPGe clover detectors were positioned in pairs at angles of 47° , 90° and 133° with respect to the incident proton beam at a distance of 13 cm from the target position.

The Si telescope was calibrated using a ^{226}Ra source which provides α particles at energies of 4.6, 4.8, 5.3, 5.5, 6.0 and 7.7 MeV. An additional 9 calibration points between 4.4 MeV and 16.1 MeV were obtained using levels populated in the $^{12}\text{C}(p,p')$ reaction. Well known levels at low excitation energy populated in the $^{152,154}\text{Sm}(p,t)$ reactions as well as the onset of the $^{152,154}\text{Sm}(p,tn)$ channels at the neutron separation energies of 7.9867(4) MeV and 8.2577(6) MeV [16], respectively, were also used. Energy deposited in adjacent rings of the Si detectors was summed and induced noise in neighbouring rings was corrected for. The energy losses due to the Al and Au dead layers of the Si detectors were calculated using the ELAST (Energy Loss And Straggling Tool) program [17] and the recoil energy imparted to the target nucleus was also accounted for. A resolution (FWHM) of 130 keV was obtained for the ground state of ^{150}Sm in the $^{152}\text{Sm}(p,t)$ reaction.

The HPGe clover detectors were calibrated using ^{22}Na , ^{54}Mn , ^{57}Co , ^{60}Co , ^{109}Cd , ^{133}Ba , ^{137}Cs and ^{152}Eu sources. The photopeak efficiency was 4.8% at 103 keV and an energy resolution of 2.6 keV and 3.5 keV (FWHM) was obtained at energies of 122 keV and 963 keV respectively.

III. TRITON PROJECTIONS AND IDENTIFICATION OF DISCRETE STATES

Energy spectra for tritons in coincidence with γ rays from the recent $^{154,156,158}\text{Gd}(p,t)$ studies by Ross *et al.* [18] and Allmond *et al.* [19] are shown in Figure 1 and compared to those obtained in the present work for the $^{152,154}\text{Sm}(p,t)$ reactions. The PLS is clearly present between 2.1-3.3 MeV excitation energy in all of these reactions. The excitation energy of the structure is plotted in Figure 2 and appears to decrease with increasing neutron number.

Particle gamma coincidences are a powerful spectroscopic tool, see for example reference [20]. A gate placed on a triton energy of interest in the $t\text{-}\gamma$ coincidence matrix corresponds to gating on a certain excitation energy in the residual nucleus. This gate returns a spectrum of γ rays that must be emitted from states at or below

this excitation energy and often enhances low intensity γ rays that are obscured in the total projection. On the other hand, gating on a γ ray in the $t\text{-}\gamma$ matrix typically gives a triton energy spectrum with a discrete peak corresponding to the direct population of the γ -ray emitting level, as well as counts at higher excitation energy which correspond to states that feed that level, both directly and indirectly. These features can be observed in the spectrum shown in Figure 3 obtained with a gate placed on the 334 keV γ ray from the transition between the first 2^+ state in ^{150}Sm and the ground state. The peak at 334 keV corresponds to direct population of the 2^+ level. Also visible are the plethora of other discrete states that are directly populated by the (p, t) reaction and then feed the 2^+ state as well as a smooth continuum region above approximately 3.5 MeV. A further example is shown in Figure 4. In panel (a) a γ -ray energy spectrum showing a section of the total γ -ray projection from the $^{152}\text{Sm}(p,t\text{-}\gamma)$ coincidence matrix is shown. In panel (b) a γ -ray energy spectrum in coincidence with tritons corresponding to an excitation energy range of 1210-1290 keV in ^{150}Sm is shown. The 922 keV γ ray is from the level at 1255 keV. The 712 keV transition is from the level at 1046 keV, which is fed by the 1255 keV level via a 209 keV transition not shown in the Figure. In panel (c) a triton energy spectrum in coincidence with the 922 keV γ ray is shown. This spectrum, typical of those observed when gating on non-yrast levels, shows the direct population peak at 1255 keV and very little feeding from higher lying excited states.

In order to identify new discrete states in $^{150,152}\text{Sm}$ a gate is first placed on a γ ray of interest in the $t\text{-}\gamma$ matrix. The approximate excitation energy of the level (typical accuracy of $\sim 20\text{-}30$ keV) is then measured by fitting the energy of the triton peak, see Figure 4, corresponding to direct population of the level. Subtracting the γ -ray energy from the excitation energy corresponding to the triton peak often identifies the level that is being fed by the transition. This can only be performed unambiguously either when there is just one possible final level within the experimental uncertainty, when multiple γ rays depopulate the level, or when the γ -ray placement can be confirmed using $t\text{-}\gamma\text{-}\gamma$ coincidences. Once the γ ray has been placed in the level scheme the γ -ray energy can be summed with the energy of the level that is being fed, which provides a much more precise measurement (typically 0.2 keV) of the excitation energy of the state of interest; see reference [20] for more details.

The levels and γ rays observed in $^{150,152}\text{Sm}$ are listed in Tables I and II, respectively. Numerous new levels and γ -ray emitting transitions were identified. In the first two columns the level energy and γ -ray energies are listed. The relative γ -ray branching for each level, expressed as a percentage of the strongest transition, is listed in the third column. In column four the triton peak energy from the present work is listed, which is obtained from fitting the peak corresponding to direct population of the level after gating on the γ ray from the same row of the table.

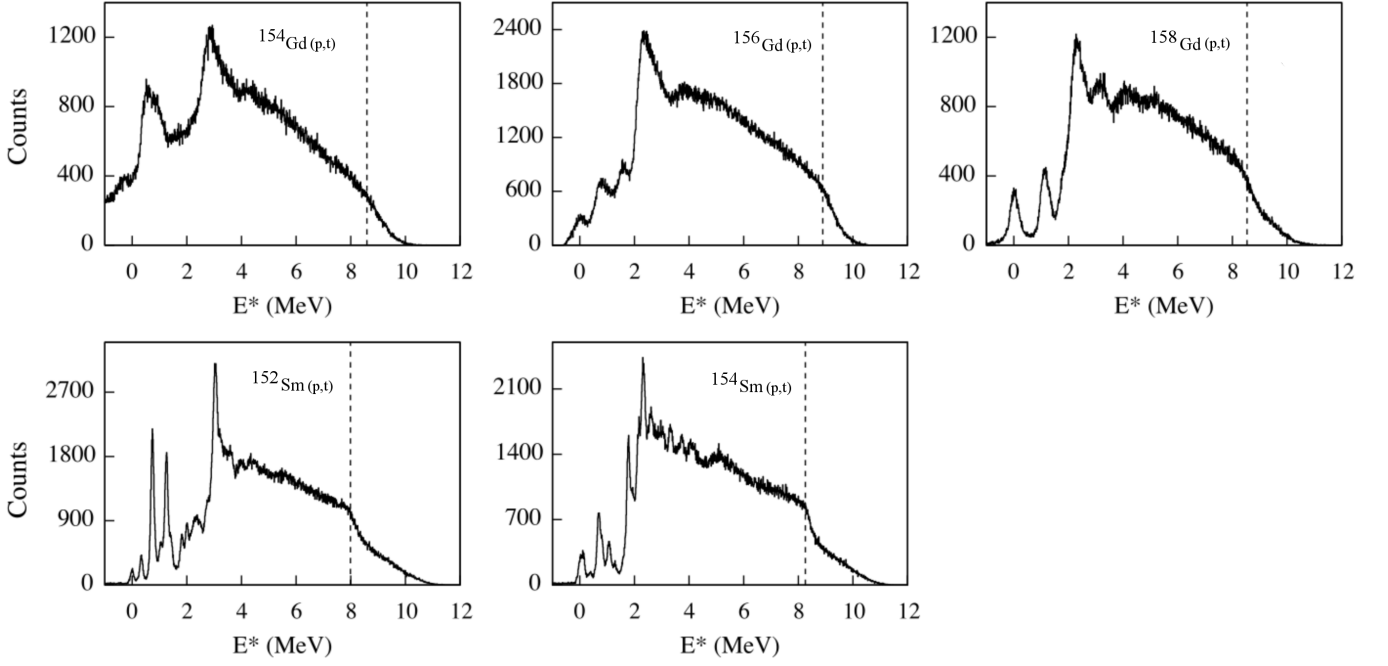


Figure 1. Triton projections of the (t,γ) matrices produced in the $^{154,156,158}\text{Gd}(p,t)$ and $^{152,154}\text{Sm}(p,t)$ reactions. The single-neutron separation energies are indicated by the dashed lines. The Gd data is from references [18, 19]. It can be seen that the energy resolution is much improved in the Sm data.

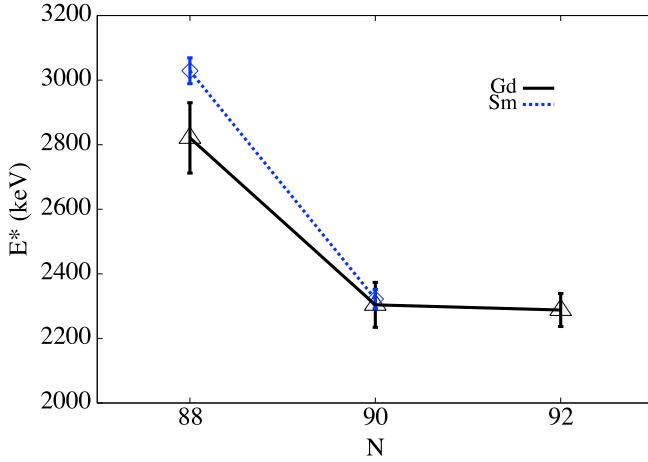


Figure 2. (Color online) The excitation energy of the PLS as a function of neutron number for the Gd (black points and solid black line) and Sm (blue points and dashed blue line) isotopes.

In the fifth column the γ -ray energy is subtracted from the triton peak energy. This can be compared with the corresponding level energy from the NNDC database [16] listed in the sixth column. In order for a definite assignment to be made, we require that these values lie within one standard deviation of each other. In the seventh column the γ -ray energy obtained in the present work is summed with the NNDC energy from column six to obtain the precise level energy. For levels which decay by

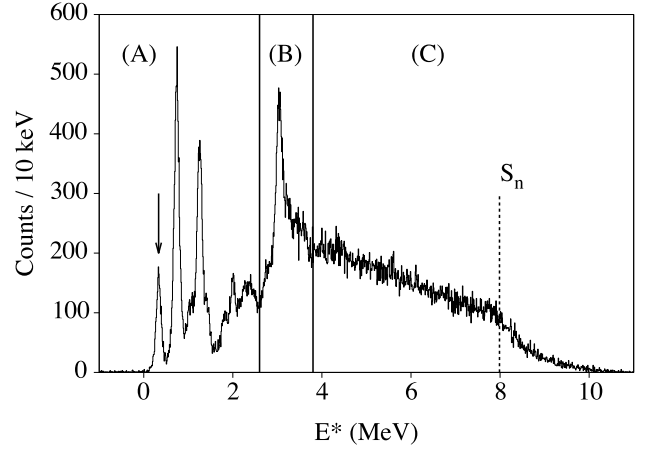


Figure 3. Triton energy spectrum in coincidence with the 334 keV γ ray transition between the first 2^+ state in ^{150}Sm and the ground state. The triton peak corresponding to direct population of the level is indicated by the arrow. In part (A) peaks corresponding to discrete states can be seen. In part (B), at intermediate excitation energy, the PLS is present. In part (C), the smoothly varying continuum region and the onset of the (p,tn) channel above the single neutron separation energy can be observed.

multiple observed γ rays, the final level energy was obtained from a weighted average of the values in column seven.

In columns eight to eleven the spin and parity, exci-

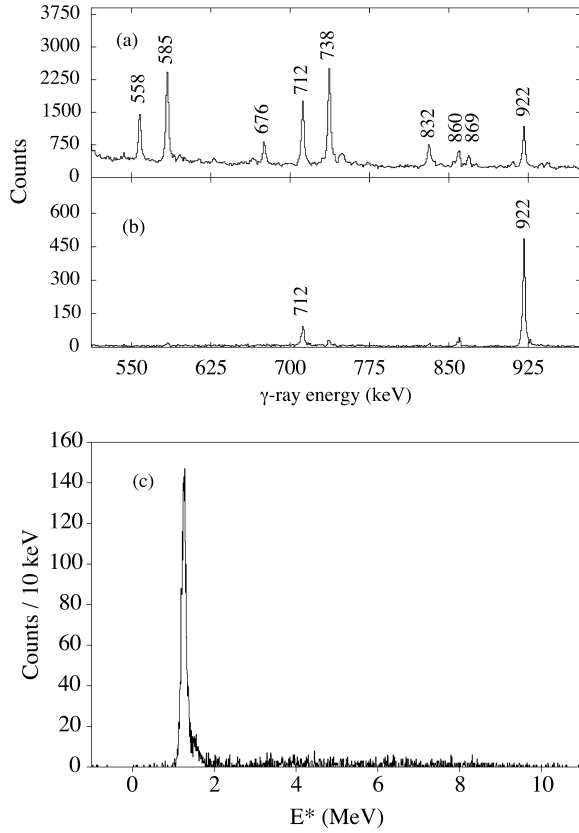


Figure 4. A γ -ray energy spectrum showing a section of the total γ -ray projection from the $^{152}\text{Sm}(p,t-\gamma)$ coincidence matrix is shown in panel (a). In panel (b) the γ -ray energy spectrum in coincidence with tritons corresponding to an excitation energy between 1210 and 1290 keV is shown. The 922 keV γ ray is from the level at 1255 keV in ^{150}Sm . The 712 keV γ is from the level at 1046 keV, which is fed by the 1255 keV level via a 209 keV transition not shown in the Figure. In panel (c) a triton energy spectrum in coincidence with the 922 keV γ ray is shown. The narrow peak corresponds to direct population of the 1255 keV level. In contrast to the 2_1^+ to ground-state transition, notice that for this non-yrast level there is comparatively little feeding from higher lying excited states.

tation energy, γ -ray energy and relative γ -ray branching from the NNDC database are listed for previously known levels to compare to the values obtained in the present work. The NNDC values for γ -ray energies and intensities are only listed for γ rays observed in the present work, the full set of known γ rays for each level can be found in reference [16].

In Figures 5 and 6 the primary γ -ray decays observed from levels directly populated in the region of the PLS for ^{150}Sm and ^{152}Sm , respectively, are shown. Newly identified levels and newly identified or newly placed γ -ray transitions are shown in red, and the region of the PLS is indicated by the dashed lines. In Figures 7 and 8 excitation energy is plotted against spin for levels directly populated in the present work. Newly identified levels

are shown in red. The horizontal lines indicate possible spin ranges for the levels based on the spins of the levels populated by their gamma-decay.

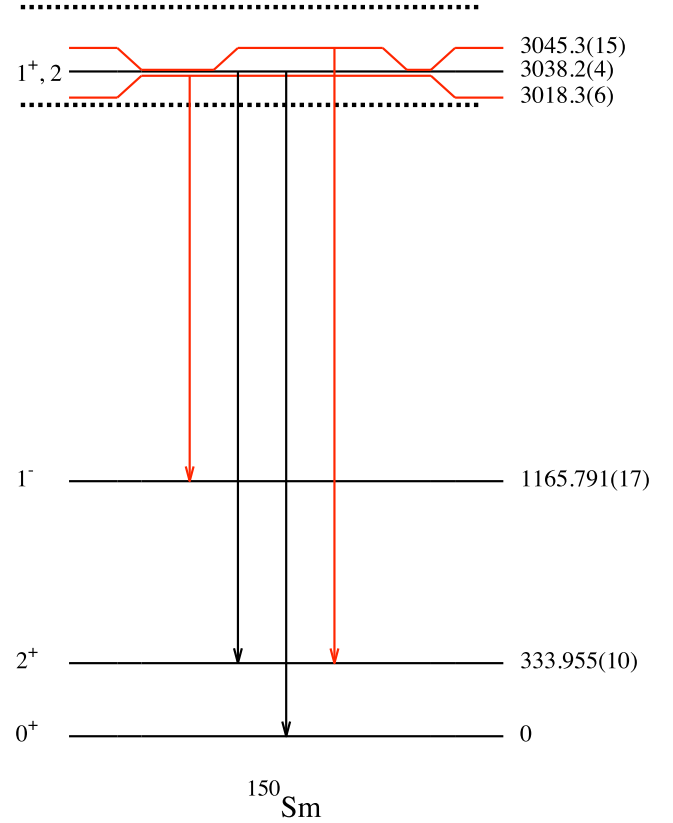


Figure 5. (Color online) Partial level scheme of ^{150}Sm showing the primary γ ray decays from levels directly populated in the $^{152}\text{Sm}(p,t)$ reaction, in the region of the PLS indicated by the dashed lines. Newly identified levels and γ rays are shown in red.

In the following sections the levels populated in ^{150}Sm and ^{152}Sm in the present work are discussed. Comments are provided only for levels for which new information was obtained or when required for a full understanding of the results presented in Tables I and II.

A. Comments on Levels and γ -ray transitions observed in ^{150}Sm

The level at 1603.1(7) keV

A 1269.1(7) keV γ -ray transition was placed between the 1603.1(7) keV and 2_1^+ levels. The cross section for the population of this level was measured by Debenham to be 0.48% of the cross section for populating the 0_2^+ level, both measurements at a laboratory angle of 25 degrees. This is consistent with the value of 0.39(14)% obtained in the present work, integrated across the entire angular

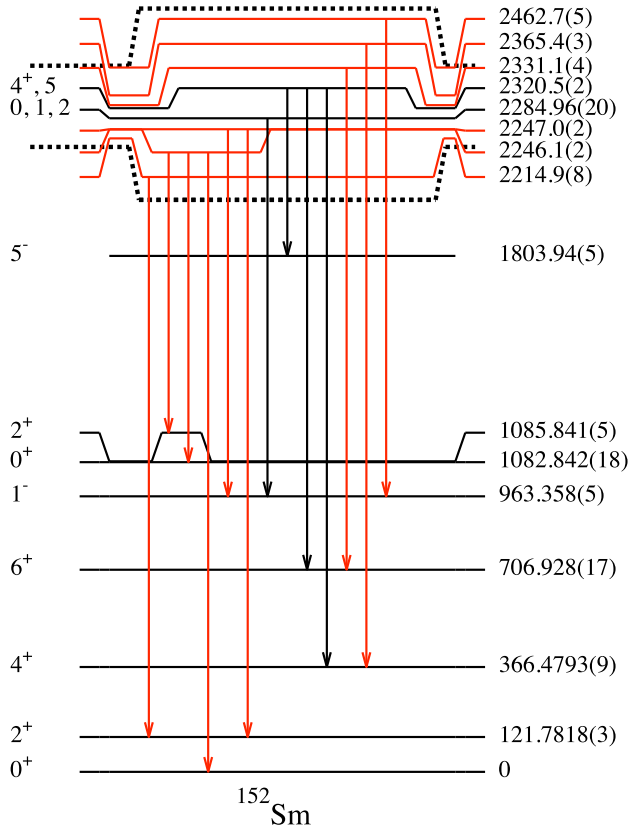


Figure 6. (Color online) Same as Figure 5 but for ^{152}Sm from the $^{154}\text{Sm}(p,t)$ reaction.

range of the telescope, and including only the strength decaying via the 1269.1(7) keV γ ray.

The level at 1794.2(2) keV

The NNDC database lists a 2^+ state at 1794.30(3) keV with four known γ rays at energies of 151.64(4), 600.43(25), 722.65(18) and 1798(4) keV. In the present work, the 1798(4) keV γ ray was not observed; it should be seen in the spectrum if the relative intensity from the literature is correct, and it is likely that this transition was misassigned. The 151.64(4) transition was also not observed, but would not be expected to be seen in the spectrum due to the low relative intensity. In addition, we assign to this level 628.5(3) keV and 1459.9(4) keV transitions.

The level at 1826.7(3) keV

A 1053.3(3) keV γ ray is newly observed in prompt coincidence with a state populated at 1824(8) keV in the particle data. This transition is assigned between a new level at 1826.7(3) keV and the 4^+ state at

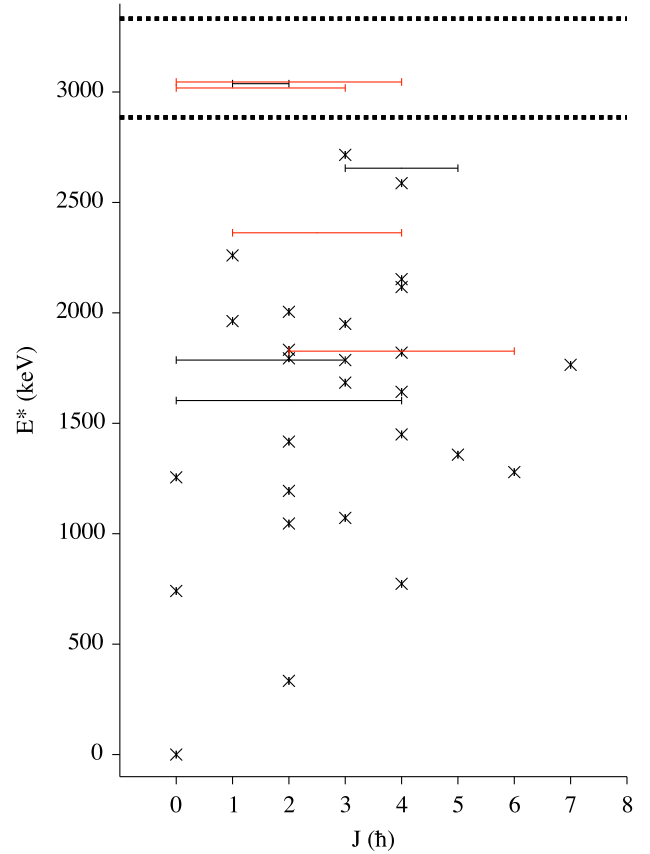


Figure 7. (Color online) A plot of excitation energy against spin for levels directly populated in ^{150}Sm . States of known spin are indicated by a black cross. Newly observed states are shown in red. States for which the spin is uncertain are plotted as horizontal lines. The range of possible spins for each level was obtained either from the literature, where available, or estimated using the observed primary γ -ray transitions by assuming that the spin of a level was within two units of angular momentum of the states it was observed to feed. The region of the PLS is indicated by the black dashed lines.

773.374(12) keV. However, there are insufficient statistics to confirm this assignment using t - γ - γ coincidences. Thus, the assignment of this level remains tentative.

The level at 1832.8(2) keV

The NNDC database lists a level at 1833.01 keV with four γ -ray transitions at energies of 667.05(3), 788, 1499.35(10) and 1833.30(15) keV. The 667.05(3) keV γ ray is listed as the strongest transition, which is in disagreement with the current work where it is observed to have 48(8)% of the strength of a 1498.7(2) keV transition. However, the 667.05(3) keV transition is multiply placed in the NNDC database and the undivided intensity is given, which explains this discrepancy.

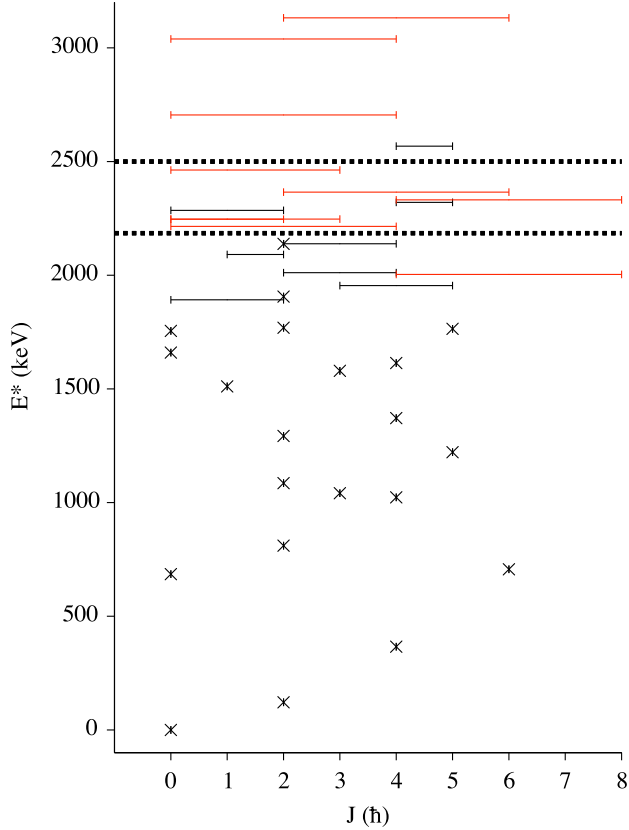


Figure 8. (Color online) Same as Figure 7 but for ^{152}Sm .

The level at 1950.2(2) keV

A 1176.8(2) keV transition is observed from the level at 1950.2(2) keV. The NNDC database makes a tentative assignment of a second γ -ray transition at 308.05(4) keV. However, energy of the state obtained in the present work is not consistent with this second transition. Therefore, we cannot confirm the assignment of the 308 keV γ ray to this level.

The level at 2260.1(3) keV

A level at 2260.1(3) keV is identified based upon a 1926.1(3) keV transition to the 2_1^+ level. Barrette *et al.* [21] reported a level at 2259.8 keV with eight decays, including a 1926.04(8) keV transition. Based upon our non-observation of the other seven γ rays reported in reference [21] it seems likely that multiple discrete states occur near 2260 keV, of which only the 2260.1(3) keV level is observed in the present work.

The level at 2362.6(2) keV

A new level is observed at an excitation energy of 2362.6(2) keV with two γ -ray transitions of 1290.9(3) and 2028.9(3) keV. The triton energy spectra gated on these two γ rays are shown in Figure 9 where the level energy obtained by summing the γ -ray energies with the NNDC energies of the lower lying levels is indicated by the blue dashed line.

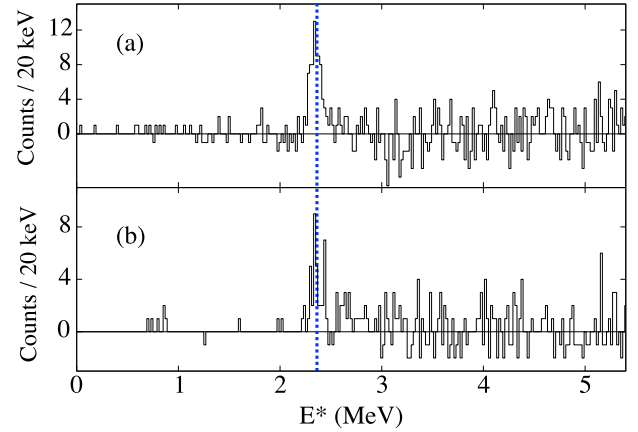


Figure 9. (Color online) Triton energy spectra obtained by gating on (a) the 1290.9(3) keV and (b) the 2028.9(3) keV γ rays showing peaks measured at 2358(8) keV and 2373(12) keV, respectively. The blue dashed line indicates the excitation energy of 2362.6(2) keV obtained by summing the γ -ray energies with the NNDC energies of the lower lying levels.

The level at 2587.2(4) keV

A new 1813.8(4) keV γ -ray transition is observed between the level at 2587.2(4) keV and the 4_1^+ state, consistent with the previous measurements of the energy of this level [22, 23]. This level is likely to be a 4^+ state based on the previous $3^+, 4^+$ assignment from reference [23] and the natural parity selection rule in the (p,t) reaction.

The level at 2654.9(7) keV

A 2320.9(7) keV transition is observed between the level at 2654.9(7) keV and the 2_1^+ state. It is possible that this is the NNDC level at 2655(7) keV [8, 22, 24, 25]. A spin and parity of $3^{(+)}, 5^{(+)}$ was previously assigned to this level [25], suggesting that the level is a 3^- state based on the transition to the 2_1^+ state and the natural parity selection rule.

B. Comments on Levels and γ -ray transitions observed in ^{152}Sm

The level at 2003.5(6) keV

A level is observed at an excitation energy of 2003.5(6) keV with a 1296.6(6) keV γ -ray transition. This state could correspond to one of three levels from the NNDC database at excitation energies of 2003.66(20), 2004.24(6) and 2004.29(11) keV. The latter two levels have known γ rays at energies of 1297.4(10) and 1297.29(13) keV respectively.

The level at 2214.9(8) keV

A new 2093.1(8) keV γ ray from the level at 2214.9(8) keV is observed. A level has previously been observed at an excitation energy of 2214.92(10) keV [26]. However, this level has been assigned as a 8^+ state which is inconsistent with the transition to the 2_1^+ state observed in the present work.

The levels at 2246.1(2) keV and 2247.0(2) keV

A level at 2246.1(2) keV is observed with three γ -ray transitions at energies of 1160.3(3), 1163.3(4) and 2245.8(8) keV. Additionally, a level at 2247.0(2) keV with two γ -ray transitions of 1283.9(4) and 2125.1(3) keV is observed. Separate level assignments are made since the level energies obtained using the 1283.9(4) and 2125.1(3) keV transitions are 3.0 and 2.7 standard deviations respectively from the level energy evaluated using the remaining three γ rays. A level at 2247.23 keV was previously observed [27] with transitions to the 0_1^+ , 2_1^+ and 1_1^- levels.

The level at 2331.1(4) keV

A 1624.2(4) keV γ ray is observed and assigned as a transition to the 6_1^+ state from the level at 2331.1(4) keV. We note that a level at 2332.42 keV has been previously observed [27] in the $(\alpha, 2n\gamma)$ reaction with transitions to the 6_1^+ and 8_1^+ levels.

The level at 2365.4(3) keV

A 1998.9(3) keV transition between the level at 2365.4(3) keV to the 4_1^+ level is observed. A level at 2365 keV has been previously observed [27] in the Coulomb excitation reaction with transitions to the 4^+ levels at 1371.735(12) and 1612.90(4) keV. These transitions, at 994 keV and 753 keV respectively, are not observed in the present work despite the higher γ -ray detection efficiency at those energies. Therefore, it is unlikely that this is the same level.

The level at 2462.7(5) keV

A 1499.3(5) keV γ ray from a level at 2462.7(5) keV is observed. A 1498.7(2) keV γ ray is also observed in the $^{152}\text{Sm}(p,t)$ reaction, but the amount of contamination is expected to be negligible. A level at 2463.17 keV was previously observed [27] in the $(n,n'\gamma)$ reaction with a transition to the 1_1^- state, which is consistent with the assignment made in the present work.

The level at 3132.0(5) keV

A new level is placed at an excitation energy of 3132.0(5) keV with a 2765.5(5) keV γ ray. The triton peak obtained by gating on this γ ray is shown in Figure 10 and compared to the level energy obtained by summing the γ -ray energy with the NNDC energy of the lower lying level.

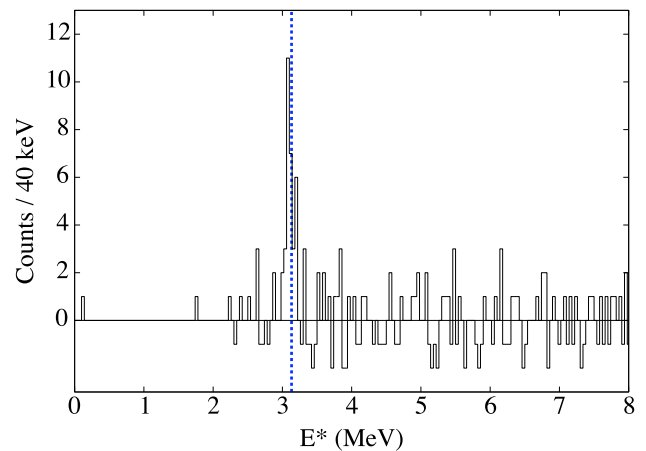


Figure 10. (Color online) Triton energy spectrum obtained by gating on the 2765.5(5) keV γ ray. The dashed blue line indicates the level energy obtained by summing the γ -ray energy with the NNDC energy of the lower lying level that is fed.

Table I: Levels and γ rays observed in the $^{152}\text{Sm}(p,t)$ reaction. Refer to the text for full description of each column. The uncertainties are indicated by the superscript. Newly identified levels and γ rays are shown in bold. A dash in columns 4 and 5 indicates that the triton peak corresponding to the direct population of the level was not measured in coincidence with the γ ray in this row. This tends to occur for levels that are strongly fed by higher lying states. In this case, a γ ray may still be placed if there are multiple observed transitions depopulating the level, or if it is a well known transition from a low lying state.

E_x (keV)	E_γ (keV)	I_γ	E_x^t (keV)	$E_x^t - E_\gamma$ (keV)	E_f^{ND} (keV)	$E_\gamma + E_f^{ND}$ (keV)	$J^{\pi, ND}$	E_x^{ND} (keV)	E_γ^{ND} (keV)	I_γ^{ND}	$\sigma_{(34^\circ - 58^\circ)}$ (% of 2_1^+)
333.7 ²	333.7 ²	100	341 ¹⁴	7 ¹⁴	0	333.7 ²	2 ⁺	333.955 ¹⁰	333.961 ¹¹	100 ³	100 ²
740.6 ²	406.6 ²	100	741 ⁴	334 ⁴	333.96	740.6 ²	0 ⁺	740.464 ¹⁹	406.508 ²²	100	282 ⁶
773.3 ³	439.3 ³	100	780 ⁵	341 ⁵	333.96	773.3 ³	4 ⁺	773.374 ¹²	439.400 ¹⁴	100	9.7 ⁸
1046.3 ²	712.4 ³ 1046.2 ²	100 6 ²	1054 ¹¹ 1031 ¹³	342 ¹¹ -15 ¹³	333.96 0	1046.4 ³ 1046.2 ²	2 ⁺	1046.148 ¹³	712.207 ¹⁴ 1046.16 ¹⁴	100 ⁶ 8.1 ⁹	32 ²
1071.7 ²	297.5 ⁵ 737.7 ²	8 ² 100	- 1070 ⁵	- 332 ⁵	773.37 333.96	1070.9 ⁵ 1071.7 ²	3 ⁻	1071.406 ¹²	298.060 ¹³ 737.457 ¹⁵	6.70 ²³ 100.0 ¹⁹	22 ²
1165.6 ²	831.6 ³ 1165.5 ³	84 ⁵ 100	- -	- -	333.96 0	1165.6 ³ 1165.5 ³	1 ⁻	1165.791 ¹⁷	831.83 ⁵ 1165.74 ³	75 ³ 100 ⁴	-
1193.9 ²	860.0 ³ 1193.8 ²	67 ⁵ 100	1193 ⁵ 1194 ⁴	332 ⁵ 0 ⁴	333.96 0	1194.0 ³ 1193.8 ²	2 ⁺	1193.843 ¹²	859.88 ³ 1193.830 ²²	73.3 ¹⁶ 100 ³	38 ²
1255.4 ¹	209.2 ² 921.5 ²	11 ¹ 100	1258 ⁴ 1259 ⁴	1049 ⁴ 338 ⁴	1046.15 333.96	1255.3 ² 1255.5 ²	0 ⁺	1255.512 ²⁰	209.364 ¹⁹ 921.55 ¹³	8.9 ¹⁶ 100 ⁷	186 ⁴
1278.9 ²	505.5 ²	100	1271 ⁷	766 ⁷	773.37	1278.9 ²	6 ⁺	1278.922 ¹⁴	505.508 ²³	100	5.5 ⁶
1357.9 ⁴	584.5 ⁴	100	1365 ⁷	781 ⁷	773.37	1357.9 ⁴	5 ⁻	1357.710 ¹³	584.274 ¹²	100 ³	6 ¹
1417.2 ²	251.2 ⁴ 345.8 ³ 1083.3 ³	48 ⁵ 100 30 ⁵	1418 ⁵ 1417 ⁴ 1427 ¹⁰	1167 ⁵ 1071 ⁴ 344 ¹⁰	1165.74 1071.41 333.96	1417.0 ⁴ 1417.2 ³ 1417.3 ³	2 ⁺	1417.346 ¹³	251.582 ¹⁹ 345.950 ¹⁷ 1083.34 ⁴	43.7 ¹⁸ 100 ¹⁰ 70 ⁸	30 ²
1449.7 ⁴	676.3 ⁴	100	1454 ¹²	778 ¹²	773.37	1449.7 ⁴	4 ⁺	1449.182 ¹³	675.853 ²⁴	100 ²	2.3 ⁶
1505.2 ⁶	1171.2 ⁶	100	-	-	333.96	1505.2 ⁶	3 ⁺	1504.572 ¹³	1170.589 ²⁴	100.0 ¹⁴	-
1603.1 ⁷	1269.1⁷	100	1610 ⁴⁰	341 ⁴⁰	333.96	1603.1 ⁷		1603 ⁴			1.1 ⁴
1642.6 ⁷	869.2 ⁷	100	1638 ²²	769 ²²	773.37	1642.6 ⁷	4 ⁺	1642.611 ¹²	869.256 ¹⁴	100 ¹	2.0 ⁵
1684.1 ³	911.0 ⁶ 1349.9 ⁴	60 ⁷ 100	1715 ²⁷ 1698 ²⁰	804 ²⁷ 348 ²⁰	773.37 333.96	1684.4 ⁶ 1683.9 ⁴	3 ⁻	1684.162 ¹⁷	910.88 ⁴ 1350.28 ¹⁰	50 ⁶ 100 ⁶	3.5 ⁶
1764.8 ³	485.9 ³	100	1783 ²⁰	1297 ²⁰	1278.92	1764.8 ³	7 ⁻	1764.89 ⁴	485.8 ³	100 ⁴	1.1 ³
1786.3 ⁵	620.5 ⁵	100	1778 ¹²	1158 ¹²	1165.79	1786.3 ⁵	(≤ 3)	1786.30 ¹³	620.40 ²⁰	95 ¹⁶	1.8 ⁵
1794.2 ²	600.5 ⁴ 628.5 ³ 722.9 ⁴ 1459.9⁴	44 ⁸ 100 56 ¹⁰ 42 ¹⁰	- 1796 ⁷ 1802 ¹² 1764 ¹⁶	- 1168 ⁷ 1079 ¹² 304 ¹⁶	1193.84 1165.79 1071.41 333.96	1794.3 ⁴ 1794.3 ³ 1794.3 ⁴ 1793.9 ⁵	2 ⁺	1794.30 ³	600.43 ²⁵ 628.56 ¹⁴ 722.65 ¹⁸	15 ³ 24 ⁴	13 ¹
1819.9 ²	748.5 ² 1485.5 ⁶	100 24 ⁸	1806 ¹² 1828 ²⁶	1058 ¹² 343 ²⁶	1071.41 333.96	1819.9 ² 1819.5 ⁶	4 ⁺	1819.510 ¹³	748.06 ⁹ 1485.50 ¹⁴	100 ² 36.7 ¹⁵	7.6 ⁹
1826.7³	1053.3³	100	1824 ⁸	771 ⁸	773.37	1826.7 ³					5.3 ⁷
1832.8 ²	667.3 ³ 1498.7 ²	48 ⁸ 100	1834 ¹⁰ 1832 ⁸	1167 ¹⁰ 333 ⁸	1165.79 333.96	1833.1 ³ 1832.7 ²	(2) ⁺	1833.01 ³	667.05 ³ 1499.35 ¹⁰	100 ⁴ 15.2 ⁷	13 ¹
1836.9 ²	558.1 ²	100	-	-	1278.92	1836.9 ²	8 ⁺	1837.03 ¹⁰	558.1 ¹	100	-
1950.2 ²	1176.8 ²	100	1960 ⁷	783 ⁷	773.37	1950.2 ²	3 ⁻	1952.46 ³	1176.6 ¹³	100 ²⁰	8.6 ⁹
1962.9 ⁷	1222.4 ⁷	100	1948 ²⁸	726 ²⁸	740.46	1962.9 ⁷	1 ⁽⁻⁾	1963.72 ⁴	1223.26 ⁸	100 ⁷	1.5 ⁵

Table I Continued:

E_x (keV)	E_γ (keV)	I_γ	E_x^t (keV)	$E_x^t - E_\gamma$ (keV)	E_f^{ND} (keV)	$E_\gamma + E_f^{ND}$ (keV)	$J^{\pi, ND}$	E_x^{ND} (keV)	E_γ^{ND} (keV)	I_γ^{ND}	$\sigma_{(34^\circ - 58^\circ)}$ (% of 2_1^+)
2004.8 ⁴	811.2 ⁶ 2004.6 ⁵	45 ¹² 100	2005 ¹⁴ 2008 ¹⁶	1194 ¹⁴ 3 ¹⁶	1193.84 0	2005.0 ⁶ 2004.6 ⁵	2 ⁺	2005.5 ⁸	812.1 ⁸		7 ¹
2117.0 ⁴	1343.6 ⁴	100	2114 ¹²	770 ¹²	773.37	2117.0 ⁴	4 ⁺	2117.030 ¹⁵	1343.78 ²²	100 ³	4.9 ⁷
2152.7 ⁴	1379.3 ⁴	100	2157 ¹⁷	778 ¹⁷	773.37	2152.7 ⁴	4 ⁺	2152.56 ³	1379.12 ⁶	100 ¹²	4.3 ⁷
2260.1 ³	1926.1 ³	100	2265 ⁹	339 ⁹	333.96	2260.1 ³	(1 ⁻)	2259.94 ⁴	1926.04 ⁸	33 ⁷	11 ¹
2362.6 ²	1290.9 ³ 2028.9 ³	66 ¹³ 100	2358 ⁸ 2373 ¹²	1067 ⁸ 344 ¹²	1071.41 333.96	2362.3 ³ 2362.9 ³					13 ¹
2587.2 ⁴	1813.8 ⁴	100	2602 ²⁴	773 ²⁴	773.37	2587.2 ⁴	3 ⁺ , 4 ⁺	2587.3 ⁵			4.3 ⁹
2654.9 ⁷	2320.9 ⁷	100	2640 ²²	319 ²²	333.96	2654.9 ⁷	(3,5)	2655 ⁷			4.0 ⁹
2715.5 ³	1521.7 ³	100	2734 ¹⁸	1212 ¹⁸	1193.84	2715.5 ³	3 ⁻	2715 ⁴			5.5 ⁸
3018.3 ⁶	1852.5 ⁶	100	3018 ¹²	1166 ¹²	1165.79	3018.3 ⁶					4.3 ⁹
3037.8 ⁹	2702.9 ¹³ 3038.5 ¹²	100 30 ⁸	3042 ⁸ 3060 ¹⁸	339 ⁸ 22 ¹⁸	333.96 0	3036.9 ¹³ 3038.5 ¹²	1,2 ⁺	3038.2 ⁴	2704.6 ⁷ 3037.8 ¹⁰	100 ⁵ 33 ¹⁷	40 ³
3045.3 ¹⁵	2711.3 ¹⁵	100	3045 ⁹	334 ⁹	333.96	3045.3 ¹⁵					38 ³

Table II: Same as Table I but for the $^{154}\text{Sm}(p,t)$ reaction. Refer to the text for full description of each column. The uncertainties are indicated by the superscript. Newly identified levels and γ rays are shown in bold.

E_x (keV)	E_γ (keV)	I_γ	E_x^t (keV)	$E_x^t - E_\gamma$ (keV)	E_f^{ND} (keV)	$E_\gamma + E_f^{ND}$ (keV)	$J^{\pi, ND}$	E_x^{ND} (keV)	E_γ^{ND} (keV)	I_γ^{ND}	$\sigma_{(34^\circ - 58^\circ)}$ (% of 2_1^+)
121.7 ²	121.7 ²	100	115 ⁸	-7 ⁸	0	121.7 ²	2 ⁺	121.7818 ³	121.7817 ³	100	100 ²
366.2 ²	244.4 ²	100	364 ⁹	119 ⁹	121.78	366.2 ²	4 ⁺	366.4793 ⁹	244.6974 ⁸	100	8.0 ⁵
685.2 ³	563.4 ³	100	681 ⁹	118 ⁹	121.78	685.2 ³	0 ⁺	684.751 ²¹	562.98 ³	100.0 ¹⁹	95 ²
706.7 ³	340.2 ³	100	704 ⁸	364 ⁸	366.48	706.7 ³	6 ⁺	706.928 ¹⁷	340.45 ³	100	6.5 ⁵
810.6 ²	443.7 ⁵ 688.8 ² 810.7 ⁴	36 ³ 100 46 ⁴	812 ⁷ 817 ⁸ 799 ⁷	368 ⁷ 128 ⁸ -12 ⁷	366.48 121.78 0	810.2 ⁵ 810.6 ³ 810.7 ⁴	2 ⁺	810.453 ⁵	444.00 ³ 688.670 ⁵ 810.451 ⁵	34.8 ¹³ 100.0 ⁶ 37.0 ³	47 ²
963.3 ³	841.5 ²	100	-	-	121.78	963.3 ³	1 ⁻	963.358 ⁵	841.570 ⁵	100.0 ¹⁸	-
1023.1 ³	656.5 ³ 901.6 ⁵	100 69 ¹⁶	1025 ¹² 1039 ¹⁴	369 ¹² 137 ¹⁴	366.48 121.78	1023.0 ³ 1023.4 ⁵	4 ⁺	1022.970 ⁵	656.489 ⁵ 901.19 ⁵	100.0 ¹⁵ 59.2 ¹⁷	5.0 ⁷
1041.2 ²	674.7 ⁴ 919.5 ³	27 ⁵ 100	1036 ¹² 1031 ⁸	361 ¹² 112 ⁸	366.48 121.78	1041.1 ⁴ 1041.3 ³	3 ⁻	1041.122 ⁴	674.65 ³ 919.337 ⁴	40.4 ⁸ 100.0 ¹⁰	13 ¹
1085.6 ²	963.7 ³ 1085.7 ³	100 57 ⁵	1082 ⁸ 1089 ⁹	118 ⁸ 3 ⁹	121.78 0	1085.5 ³ 1085.7 ³	2 ⁺	1085.841 ⁵	964.057 ⁵ 1085.837 ¹⁰	100.00 ²⁴ 69.71 ¹⁰	42 ²
1125.3 ³	418.4 ³	100	-	-	706.93	1125.3 ³	8 ⁺	1125.39 ³	418.45 ³	100	-
1221.6 ³	855.1 ³	100	1214 ¹¹	359 ¹¹	366.48	1221.6 ³	5 ⁻	1221.64 ³	855.21 ⁷	100 ³	3.5 ⁵
1233.9 ²	867.9 ⁴ 1112.0 ²	46 ⁸ 100	- -	- -	366.48 121.78	1234.4 ⁴ 1233.8 ²	3 ⁺	1233.863 ³	867.380 ³ 1112.076 ³	30.93 ¹⁸ 100.0 ⁵	-
1293.0 ¹⁴	926.5 ¹⁴	100	1276 ¹⁵	350 ¹⁵	366.48	1293.0 ¹⁴	2 ⁺	1292.773 ¹⁰	926.29 ⁴	100.0 ¹²	2.2 ⁵
1310.5 ³	603.6 ³	100	-	-	706.93	1310.5 ³	6 ⁺	1310.505 ²²	603.56 ³	100 ⁴	-
1371.7 ³	1005.2 ⁶	100	1393 ²²	388 ²²	366.48	1371.7 ³	4 ⁺	1371.735 ¹²	1005.27 ⁵	100.0 ¹⁶	3.2 ⁵
1505.9 ³	799.0 ³	100	-	-	706.93	1505.9 ³	7 ⁻	1505.77 ³	798.82 ³	100 ³	-
1510.9 ⁴	1389.1 ⁴	100	1542 ²⁰	153 ²⁰	121.78	1510.9 ⁴	1 ⁻	1510.790 ²⁵	1389.03 ⁴	100.0 ²¹	1.6 ⁵

Table II Continued:

E_x (keV)	E_γ (keV)	I_γ	E_x^t (keV)	$E_x^t - E_\gamma$ (keV)	E_f^{ND} (keV)	$E_\gamma + E_f^{ND}$ (keV)	$J^{\pi, ND}$	E_x^{ND} (keV)	E_γ^{ND} (keV)	I_γ^{ND}	$\sigma_{(34^\circ - 58^\circ)}$ (% of 2_1^+)
1559.6 ³	1193.1 ³	100	-	-	366.48	1559.6 ³	5 ⁺	1559.62 ³	1193.10 ⁵	100 ³	-
1579.4 ²	1212.9 ² 1457.4 ⁴	100 42 ¹⁰	1577 ⁹ 1574 ¹⁸	364 ⁹ 117 ¹⁸	366.48 121.78	1579.4 ² 1579.2 ⁴	3 ⁻	1579.429 ¹¹	1212.948 ¹¹ 1457.643 ¹¹	100.0 ⁴ 35.13 ²⁶	8 ¹
1609.0 ⁴	483.6 ⁴	100	-	-	1125.39	1609.0 ⁴	10 ⁺	1609.26 ⁴	483.86 ³	100	-
1613.8 ⁴	906.9 ⁴	100	1618 ¹⁶	711 ¹⁶	706.93	1613.8 ⁴	4 ⁺	1612.90 ⁴	906.06 ¹⁰	100 ⁵	1.4 ⁴
1659.8 ³	696.4 ³	100	1680 ¹²	984 ¹²	963.36	1659.8 ³	0 ⁺	1658.80 ²⁵	695.9 ³	100 ⁵	7 ¹
1728.2 ⁵	1021.3 ⁵	100	-	-	706.93	1728.2 ⁵	6 ⁺	1728.27 ³	1021.41 ⁴	100 ³	-
1755.1 ²	791.7 ²	100	1772 ¹²	980 ¹²	963.36	1755.1 ²	0 ⁺	1754.98 ⁴	791.67 ⁷	100 ⁵	9.8 ⁸
1764.3 ³	1057.2 ⁵ 1398.0 ⁴	68 ²⁰ 100	1764 ¹⁹ 1775 ¹⁸	707 ¹⁹ 377 ¹⁸	706.93 366.48	1764.1 ⁵ 1764.5 ⁴	5 ⁻	1764.32 ⁵	1057.36 ⁶ 1397.88 ⁷	100 ⁶ 82 ⁵	3.2 ⁷
1769.0 ¹	397.5 ⁵ 535.2 ³ 683.9 ⁸ 728.3 ⁵ 805.5 ⁶ 958.5 ³ 1084.5 ² 1646.7 ³ 1768.9 ²	5 ² 12 ² 25 ³ 58 ⁶ 68 ⁶ 100 79 ⁶ 36 ⁵ 68 ⁸	- 1796 ⁸ - 1773 ⁴ 1760 ⁸ 1777 ⁴ - 1781 ⁹ 1779 ⁸	- 1261 ⁸ - 1045 ⁴ 955 ⁸ 819 ⁴ - 134 ⁹ 10 ⁸	1371.74 1233.86 1085.84 1041.12 963.36 810.45 684.75 121.78 0	1769.2 ⁵ 1769.1 ³ 1769.7 ⁸ 1769.4 ⁵ 1768.9 ⁶ 1769.0 ³ 1769.3 ² 1768.5 ³ 1768.9 ²	2 ⁺	1769.132 ²³	397.75 ²⁶ 535.44 ¹² 683.25 ⁹ 728.03 ⁴ 805.71 ⁹ 958.63 ⁵ 1084.36 ¹⁴ 1647.44 ¹² 1769.09 ⁵	1.9 ³ 8.8 ⁷ 24.1 ¹⁴ 56.5 ¹⁹ 77 ³ 100 ⁶ 54 ⁴ 36.9 ¹⁸ 47.3 ¹¹	141 ⁵
1879.5 ³	754.1 ³	100	-	-	1125.39	1879.5 ³	9 ⁻	1879.14 ⁴	753.83 ³	100 ³	-
1891.9 ⁴	928.5 ⁴	100	1899 ⁵	971 ⁵	963.36	1891.9 ⁴	0 ⁺ , 1, 2	1892.48 ⁵	929.12 ⁵	100 ¹⁰	21 ¹
1906.0 ²	821.6 ¹¹ 942.4 ³ 1784.5 ³ 1905.9 ³	27 ¹² 51 ¹² 100 96 ²⁰	1910 ¹² 1890 ¹⁰ 1923 ¹³ 1911 ¹⁰	1088 ¹² 948 ¹⁰ 139 ¹³ 5 ¹⁰	1085.84 963.36 121.78 0	1907.4 ¹¹ 1905.8 ³ 1906.3 ³ 1905.9 ³	2 ⁺	1906.13 ³	820.31 ⁷ 942.85 ⁶ 1784.27 ⁷ 1906.14 ⁷	8.5 ¹² 100 ⁸	29 ²
1954.5 ⁷	913.4 ⁷	100	1940 ¹²	1027 ¹²	1041.12	1954.5 ⁷	3 ⁻ , 4, 5 ⁻	1954.30 ⁵	913.17 ⁶	100 ⁵	2.8 ⁵
2003.5⁶	1296.6⁶	100	2010 ²⁰	713 ²⁰	706.93	2003.5 ⁶					2.3 ⁵
2011.1 ³	1644.6 ³ 1889.4 ⁶	70 ¹⁰ 100	2022 ¹⁰ 2010 ¹⁰	377 ¹⁰ 121 ¹⁰	366.48 121.78	2011.1 ³ 2011.2 ⁶	2 ⁺ , 3, 4 ⁺	2011.84 ⁵	1645.30 ¹⁰ 1889.95 ⁶	100 ⁹ 50 ⁹	19 ²
2091.1 ²	1050.1 ³ 1127.6 ³	99 ²⁹ 100	2092 ¹⁰ 2095 ¹¹	1042 ¹⁰ 967 ¹¹	1041.12 963.36	2091.2 ³ 2091.0 ³	1 ⁻ , 2	2091.21 ⁴	1050.10 ⁵ 1127.84 ⁵	100 ⁷ 82 ⁷	8 ¹
2138.0 ²	1096.9 ²	100	2138 ¹¹	1041 ¹¹	1041.12	2138.0 ²	2 ⁺	2138.17 ¹²	1096.96 ¹²	100 ⁴	7 ²
2138.5 ⁸	2016.7 ⁸	100	2120 ⁴⁰	103 ⁴⁰	121.78	2138.5 ⁸	(2 ⁺ , 3, 4 ⁺)	2137.92 ⁶	2016.17 ⁷		2.3 ⁷
2214.9⁸	2093.1⁸	100	2202 ²⁶	109 ²⁶	121.78	2214.9 ⁸					6 ¹
2246.1²	1160.3³ 1163.3⁴ 2245.8⁸	100 77 ²⁴ 41 ¹²	2249 ⁶ 2245 ⁸ 2234 ²⁴	1089 ⁶ 1082 ⁸ -15 ²⁴	1085.84 1082.84 0	2246.1 ³ 2246.1 ⁴ 2245.8 ⁸					24 ²
2247.0²	1283.9⁴ 2125.1³	100 95 ²⁸	2249 ⁸ 2262 ¹⁸	965 ⁸ 137 ¹⁸	963.36 121.78	2247.3 ⁴ 2246.9 ³					14 ¹
2285.2 ³	1321.8 ³	100	2296 ³⁰	974 ³⁰	963.36	2285.2 ³	0, 1, 2	2284.96 ²⁰	1321.6 ²		6.3 ⁸
2320.5 ²	516.9 ³ 1613.2 ⁴ 1953.8 ³	100 9 ³ 29 ⁵	2323 ⁹ 2288 ¹⁹ 2324 ¹⁰	1806 ⁹ 675 ¹⁹ 370 ¹⁰	1803.94 706.93 366.48	2320.8 ³ 2320.1 ⁴ 2320.3 ³	4 ⁺ , 5	2320.35 ²³	516.3 ⁴ 1613.4 ⁶ 1953.7 ⁴	100 ¹⁰ 13 ³ 30 ⁷	47 ³
2331.1⁴	1624.2⁴	100	2348 ¹⁸	724 ¹⁸	706.93	2331.1 ⁴					6.4 ⁹
2365.4³	1998.9³	100	2369 ¹³	370 ¹³	366.48	2365.4 ³					8 ¹
2462.7⁵	1499.3⁵	100	2456 ¹²	957 ¹²	963.36	2462.7 ⁵					3.5 ⁶
2567.8 ⁷	2201.3 ⁷	100	2566 ²⁰	365 ²⁰	366.48	2567.8 ⁷	4 ⁺ , 5	2567.06 ¹⁷	2200.7 ²	100 ¹⁷	3.1 ⁹

Table II Continued:

E_x (keV)	E_γ (keV)	I_γ	E_x^t (keV)	$E_x^t - E_\gamma$ (keV)	E_f^{ND} (keV)	$E_\gamma + E_f^{ND}$ (keV)	$J^{\pi, ND}$	E_x^{ND} (keV)	E_γ^{ND} (keV)	I_γ^{ND}	$\sigma_{(34^\circ-58^\circ)}$ (% of 2_1^+)
2705.0 ⁸	2583.2 ⁸	100	2702 ¹¹	119 ¹¹	121.78	2705.0 ⁸					5 ¹
3039.1 ⁸	2917.3 ⁸	100	3038 ¹⁸	121 ¹⁸	121.78	3039.1 ⁸					7 ²
3132.0 ⁵	2765.5 ⁵	100	3134 ¹²	369 ¹²	366.48	3132.0 ⁵					9 ³

IV. PARTIAL CROSS SECTIONS

Relative partial cross sections for the direct population of states in $^{150,152}\text{Sm}$ via the (p,t) reaction were obtained by gating on the γ rays listed in Tables I and II and measuring the area of the triton peak corresponding to the direct population of a level. The γ -ray detection efficiency and, when possible, the internal conversion coefficient for the γ -ray transition were accounted for. The missing strength due to unobserved γ rays and the finite angular coverage of the Si telescope were not corrected for and therefore these values should be considered as partial cross sections, averaged over the angular range of the telescope of 34 to 58 degrees. The values are given as a percentage of the cross section for direct population of the 2_1^+ level. The relative partial cross sections are listed in Tables I and II and plotted in Figures 11 and 12 where they are compared to the triton projections of the t- γ coincidence matrices for the $^{152}\text{Sm}(p,t)$ and $^{154}\text{Sm}(p,t)$ reactions, respectively. Overall the correspondence between the two is very good.

Cross sections for populating excited states in $^{150,152}\text{Sm}$ via the (p,t) reaction have previously been measured in references [9–12]. In Table III the relative cross sections obtained in the present work for the $^{152}\text{Sm}(p,t)$ reaction are compared to those obtained by Debenham *et al.* [11] and McLatchie *et al.* [10]. Since the cross sections obtained in the present work are angle averaged between 34 to 58 degrees whereas the values quoted by Debenham are the maximum differential cross sections at the listed angle, this table is provided as a general comparison only. It should be reemphasized that the values quoted in the present work are lower limits of the relative cross section if there are unobserved γ -ray decay branches. An incident proton energy of 19 MeV was used by Debenham. McLatchie quotes the differential cross section at 22.5° and used an incident proton energy of 20.6 MeV.

Overall the agreement between the three data sets is good. It can be seen that the excited 0^+ states at 740.6(2) and 1255.4(1) keV have particularly large cross sections in all three sets of measurements. This has been interpreted in terms of shape coexistence and the rapid onset of deformation that occurs in this region [7, 28].

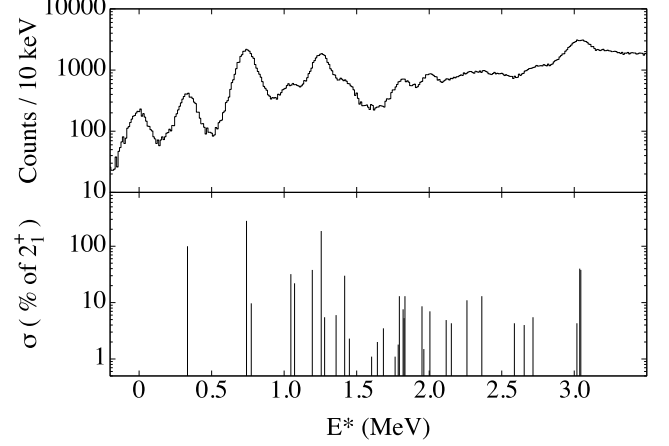


Figure 11. (Top) The triton energy projection from the $^{152}\text{Sm}(p,t\gamma)$ coincidence matrix. (Bottom) The relative partial cross sections from Table 1 are plotted.

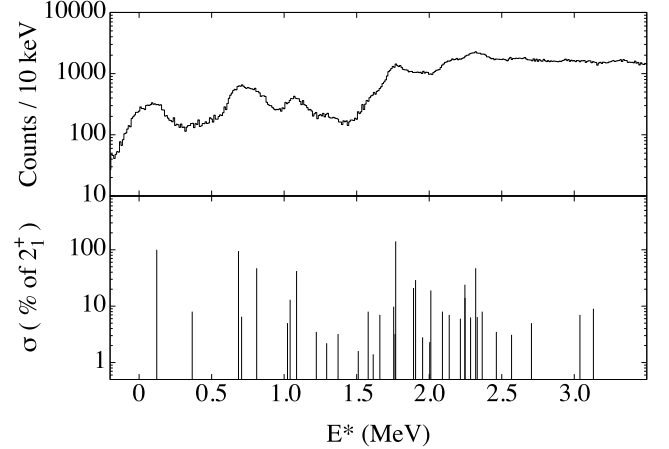


Figure 12. Same as Figure 11 but for the $^{154}\text{Sm}(p,t)$ reaction.

V. ANGULAR DISTRIBUTIONS

A. Discrete States

By measuring the angular distribution of the outgoing tritons the orbital angular momentum transfer can be determined by comparison to distributions obtained from DWBA calculations. For example, in Figure 13 the experimental angular distributions from the population of the 334 (2^+), 740 (0^+), 1256 (0^+) and 1417 (2^+) keV

Table III. The relative partial cross sections for levels in ^{150}Sm obtained in the present work are compared to the cross sections obtained by Debenham [11] and McLatchie [10]. The value reported by Debenham is the maximum differential cross section at the angle listed in the following column. All values are quoted relative to the 2_1^+ level at 333.7(2) keV, which has been scaled to 100. Debenham reports a relative error of 6.9%.

E_x (keV)	J^π	$\sigma(34^\circ - 58^\circ)$ Present work	$\sigma(\theta)_{max}$ Reference [11]	θ (degrees)	$\sigma(22.5^\circ)$ Reference [10]
333.7(2)	2^+	100(2)	100	10	100
740.6(2)	0^+	282(6)	260	25	340
773.3(3)	4^+	9.7(8)	9.9	10	<20
1046.3(2)	2^+	32(2)	42	10	<20
1071.7(2)	3^-	22(2)	5.6	35	40
1193.9(2)	2^+	38(2)	46	10	80
1255.4(1)	0^+	186(4)	170	25	180
1357.9(4)	5^-	6(1)	1.9	20	<20
1417.2(2)	2^+	30(2)	27	10	30
1449.7(4)	4^+	2.3(6)	3.7	12.5	<20
1603.1(7)		1.1(4)	1.2	25	
1642.6(7)	4^+	2.0(5)	1.2	10	
1794.2(2)	2^+	13(1)	17	10	
1832.8(2)	$(2)^+$	7.6(9)	6.8	20	<20
1950.2(2)	3^-	8.6(9)	3.7	35	<20

levels are compared to DWBA calculations produced using the DWUCK4 code [29] for $L = 0$ and 2 transfer, respectively. The optical model potential used in the present work is defined in reference [30]. The proton potential from reference [30] was used and the triton and neutron parameters were obtained from reference [31]. These parameters are listed in Table IV. The experimental angular distributions were produced by gating on the primary γ -ray transitions from those levels, and measuring the angular distribution of the outgoing tritons in the Si telescope. For levels with multiple observed γ rays the angular distributions obtained from each γ -ray gate were summed. It can be seen from Figure 13 that the theoretical curves calculated assuming the NNDC J assignments are in good agreement with the experimental data.

The level at 2320 keV was previously assigned $J = 4^+, 5$ in the NNDC database based on its γ -ray decay scheme. The angular distribution for this level is plotted in Figure 14 where it is compared to the DWBA calculations for $L=4$ and $L=5$ transfer. The reduced χ^2 for the $L=4$ and $L=5$ curves are 2.1 and 2.2 respectively, therefore a definitive assignment cannot be made.

B. The Peak-Like Structures

In panel (a) of Figure 15 the angular distribution of the PLS observed in ^{150}Sm , centered at ~ 3 MeV, is compared to the angular distribution for the background under the PLS and to the continuum region at higher excitation energy between 3.3 and 4 MeV. The error bars represent the statistical uncertainty only. The angular distribution for the PLS was obtained by measuring the strength built upon a smooth continuum background, illustrated in Figure 16, for each ring-sector pixel of the Si telescope. The angular distribution for the background

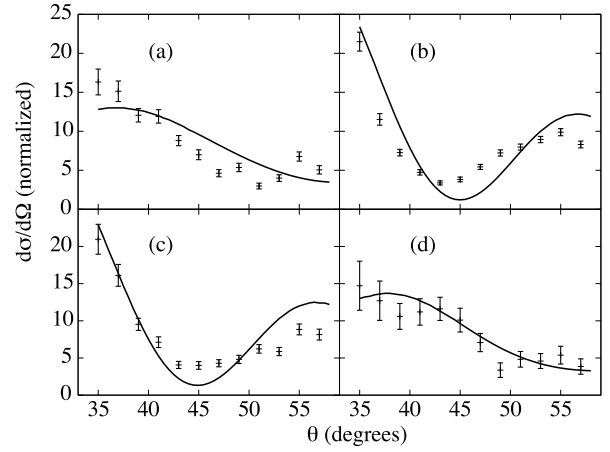


Figure 13. Experimental angular distributions (black points with error bars) obtained by gating on primary γ rays from the levels populated in the $^{152}\text{Sm}(p,t)$ reaction at (a) 334 keV, $J = 2$ (b) 740 keV, $J = 0$ (c) 1256 keV, $J = 0$ and (d) 1417 keV, $J = 2$ are compared to DWBA calculations for $L=0$ and 2 transfer (solid lines).

under the PLS was obtained from the area under the blue shaded region, for each pixel. In panel (b) the angular distributions for the PLS and background in ^{152}Sm are similarly compared to the nearby continuum region between 2.5 and 3.0 MeV.

It can be seen in panels (a) and (b) that the angular distributions of the PLS are significantly different from the distributions obtained from the nearby continuum region, and that the angular distributions obtained for the background under the PLS are very similar to the distributions obtained for the continuum region. In panel (c) of Figure 15 the angular distributions of the PLS ob-

Table IV. Optical model parameters used in the DWBA calculations. The optical model potential used in the present work is defined in reference [30]. The proton parameters are from reference [30]. The triton and neutron parameters were obtained from reference [31].

	V_r (MeV)	W' (MeV)	W_0 (MeV)	V_{so} (MeV)	R_r (fm)	R_{is} (fm)	R_{iv} (fm)	R_{so} (fm)	a_r (fm)	a_{is} (fm)	a_{iv} (fm)	a_{so} (fm)	R_c (fm)	n/c
p	57.5	29.6	3	5.65	1.200	1.150	1.259	1.010	0.670	0.779	0.76	0.75	1.25	0.85
t	160.03		17.83		1.200		1.400		0.720		0.84		1.30	0.25
n				$\lambda=25$	1.17				0.75					

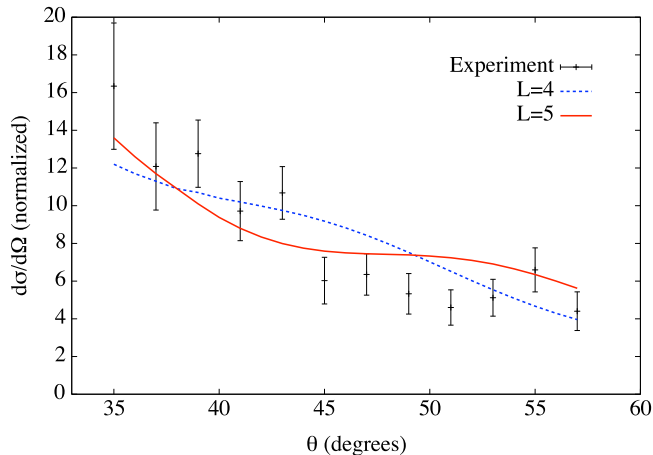


Figure 14. (Color online) The experimental angular distribution for the level at 2320.5(2) keV is compared to the DWBA calculations for $L=4$ (dashed blue line) and $L=5$ (solid red line) transfer.

served in ^{150}Sm and ^{152}Sm are compared. Despite the fact that the two PLS in the two nuclei are 700 keV apart in excitation energy the two distributions are extremely similar. This suggests that the distributions of orbital angular momentum transfers are similar in both reactions when populating the PLS. In panel (d) the angular distributions for the PLS are compared to the DWBA calculations which are most similar to the experimental data. The experimental distributions are most similar to the calculations for $L=2, 3$ and 4 transfer, which are plotted as the blue, black and red lines respectively, calculated for the $^{152}\text{Sm}(p,t)$ reaction.

VI. DISCUSSION AND SUMMARY OF RESULTS

Perhaps the most striking feature observed in the (p,t) spectra, Figure 1, is the large PLS observed in all five Sm and Gd nuclei between 2 - 3 MeV excitation energy. There, a rapid increase in the triton intensity occurs and the smooth continuum 'background' begins. Figure 2 shows that the energy of the PLS decreases with increasing neutron number, and that the structure is located at approximately the same excitation energy in Sm and Gd nuclei with the same neutron numbers. One hypoth-

esis is that the structure is partially composed of states formed by the coupling of a neutron hole near the Fermi surface to a deep lying neutron hole. Then, the energy of the structure is expected to decrease with increasing deformation, i.e. as one moves away from the $N=82$ spherical shell gap. This deep-hole, valence-hole hypothesis has previously been suggested as an explanation for broad structures observed between 7-9 MeV in the $^{112,116,118,120,122,124}\text{Sn}(p,t)$ reactions [32]. Although it was initially suggested that these structures were formed by creating two deep-lying holes below the shell closure [33], it was found that the energy systematics were better described by the coupling of a valence hole to a deep hole [34]. It has also been shown in the review by Crawley [35] that bumps observed in two neutron transfer reactions in the Cd isotopes are likely to correspond to a valence-hole deep-hole configuration. In the (p,t) study by Nakagawa *et al.* [36] bumps at lower and higher excitation energy, corresponding to valence-deep and deep-deep hole states respectively, were observed across a wide range of nuclei from ^{66}Zn to ^{230}Th . This includes one isotope of samarium, ^{148}Sm , where a bump corresponding to the deep-deep configuration was observed at an excitation energy of approximately 6 MeV. The bump corresponding to the valence-deep configuration would be expected to lie at lower excitation energy. However, it must be noted that the FWHM of these structures in the $N=82$ region is approximately 5 MeV, much larger than the narrow structures observed in the present work. A study of two-neutron hole strength in $^{142,146,148,150,152}\text{Sm}$ was performed by Struble *et al.* [13] where the broad structure observed by Nakagawa at 6 MeV in ^{148}Sm was also observed. The PLS observed in the present work can be seen in Figure 4 of that paper labelled as peak *e*. It was suggested by Struble that these much narrower structures are associated with two-hole strength in strongly up-sloping orbitals from below the $N=82$ shell closure.

In ^{152}Sm between 2.2 and 2.5 MeV, i.e. in the region of the PLS, a total of 8 levels are found which are directly populated in the (p,t) reaction including 6 newly identified levels. The majority of likely spin values for these also range from 0 to 5 \hbar . In ^{150}Sm the PLS is observed at a higher excitation energy, extending from 2.9 to 3.3 MeV. Only three discrete levels, including 2 newly identified ones, are observed in this energy region, see Figure 5. This is due in part to the lower detection efficiency for higher energy γ rays. Possible spin values for these levels lie in the 0 - 4 \hbar range, see Figure 7.

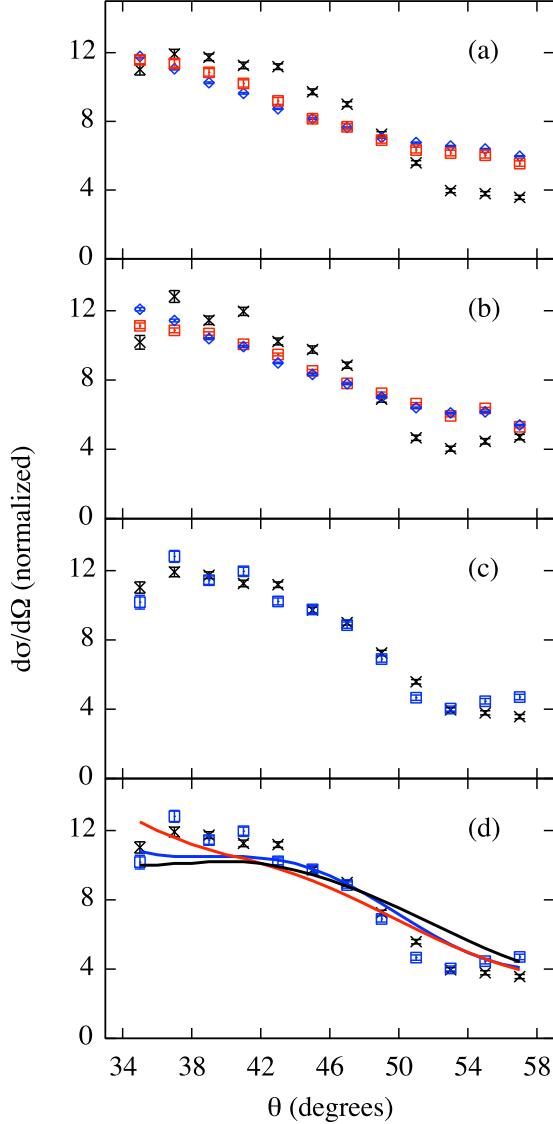


Figure 15. (Color online) In panel (a) the angular distribution of the PLS in ^{150}Sm (black points) is compared to the angular distribution for the background under the PLS (red points) and the distribution obtained for the nearby continuum region between 3.3 and 4.0 MeV (blue points). In panel (b) the angular distribution of the PLS in ^{152}Sm (black points) is compared to the angular distribution for the background under the PLS (red points) and the distribution obtained for the nearby continuum region between 2.5 and 3.0 MeV (blue points). In panel (c) the angular distributions of the PLS observed in ^{150}Sm (black points) and ^{152}Sm (blue points) are compared. Panel (d) is the same as panel (c), except that the DWBA calculations for $L=2$ (blue line), $L=3$ (black line) and $L=4$ (red line) transfer, calculated for the $^{152}\text{Sm}(p,t)$ reaction, are also plotted.

In ^{150}Sm the relative cross-section, within the angular

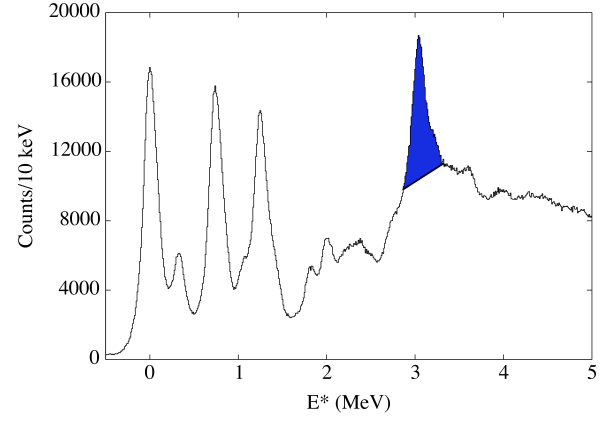


Figure 16. (Color online) The triton singles spectrum from the $^{152}\text{Sm}(p,t)$ reaction. The blue shaded area corresponds to the counts considered to belong to the PLS when measuring the angular distributions shown in panel (c) of Figure 15.

range of the telescope, for the population of the PLS, measured in the triton singles spectrum, is 213(20)% of the cross section for the direct population of the 2_1^+ level. Of this strength, 39(4)% can be accounted for by the discrete states observed in the present work. In ^{152}Sm the strength of the PLS was observed to be 117(19)% of the 2_1^+ level. Of this strength, 93(15)%, could be accounted for by the discrete states observed in the present work. This measurement is consistent with the spectrum seen in the top panel of Figure 1. from reference [12]. There, it can be seen that the region of the PLS around 2.3 MeV in ^{152}Sm appears to be dominated by a relatively small number of states with large cross sections, in particular the level measured by Saha at excitation energy of 2268 keV. This corresponds to the levels measured at 2246.1(2) keV and 2247.0(2) keV in the present work, as the excitation energies reported by Saha appear to be systematically too high.

The angular distributions of the PLS, shown Figure 15, are significantly different to that of the nearby continuum region, and have a shape more characteristic of the single L-transfer curves. This suggests that the L-transfer distribution when populating the PLS is significantly different than when populating the adjacent continuum region, and supports the conclusion that the structures are dominated by a relatively low number of states of similar spins. The fact that the angular distributions of the PLS populated in the two reactions are very similar, as shown in panel (c) of Figure 15, suggests that the L-transfer distributions are also similar.

In summary, numerous new levels and γ -ray transitions were identified in $^{150,152}\text{Sm}$ utilizing the t - γ coincidence technique, including in the region of the PLS observed between 2.3-3.0 MeV. These structures appear to be dominated by a relatively small number of discrete states, particularly in ^{152}Sm . The angular distributions of the outgoing tritons populating the PLS in the $^{152,154}\text{Sm}(p,t)$ reactions are very similar, and significantly different from

the angular distributions obtained by gating on the adjacent higher excitation energy continuum region.

VII. ACKNOWLEDGEMENTS

The authors are grateful to Professor J.L. Wood for information on levels and γ -ray transitions in ^{152}Sm and for helpful discussion of the data. This material is based

upon work supported by the U.S. Department of Energy, Office of Science, Office of Nuclear Physics under Grant Nos. DE-SC0014277, DE-FG02-05ER41379 and DE-FG02-93ER40773, by the U.S. Department of Energy, National Nuclear Security Administration under Grant Nos. DE-NA0002914 DE-NA0001801 and DE-FG52-09NA29467, by the National Science Foundation under contract PHY-130581, and by the U.S. Department of Energy NNSA Office of Defense Nuclear Nonproliferation Research & Development under Contract No. DE-AC52-07NA27344 (Lawrence Livermore National Laboratory).

-
- [1] D. A. Meyer *et al.*, Physical Review C **74**, 044309 (2006).
 - [2] N. V. Zamfir, Jing-ye Zhang, and R. F. Casten, Physical Review C **66**, 057303 (2002).
 - [3] D. Tonev *et al.*, Physical Review C **69**, 034334 (2004).
 - [4] R. F. Casten *et al.*, Physical Review C **57**, R1553 (1998).
 - [5] F. Iachello, N. V. Zamfir, and R. F. Casten, Physical Review Letters **81**, 1191 (1998).
 - [6] P. E. Garrett *et al.*, Physical Review Letters **103**, 062501 (2009).
 - [7] J. R. Maxwell, G. M. Reynolds, and N. M. Hintz, Physical Review **151**, 1000 (1966).
 - [8] J. H. Bjerregaard, O. Hansen, O. Nathan, and S. Hinds, Nuclear Physics **86**, 145 (1966).
 - [9] W. Oelert, G. Lindström, and V. Riech, Nuclear Physics A **233**, 237 (1974).
 - [10] W. McLatchie, W. Darcey, and J. E. Kitching, Nuclear Physics A **159**, 615 (1970).
 - [11] P. Debenham and N. M. Hintz, Nuclear Physics A **195**, 385 (1972).
 - [12] A. Saha, O. Scholten, D. C. J. M. Hageman, and H. Fortune, Physics Letters **85B**, 215 (1979).
 - [13] G. L. Struble *et al.*, Phys. Rev. C **23**, 2447 (1981).
 - [14] H. J. Riezebos, R. De Leo, P. B. Goldhoorn, M. N. Harakeh, and L. W. Put, Physics Letters **118B**, 287 (1982).
 - [15] S. R. Leshner *et al.*, Nucl. Instrum. Methods. Phys. Res. A **621**, 286 (2010).
 - [16] Evaluated Nuclear Structure Data File (ENSDF) - National Nuclear Data Center (NNDC), Brookhaven National Laboratory, 2014.
 - [17] Energy loss and Straggling Tool (ELAST), [Adapted from the computer program ENELOSS, written by H. Ernst (1981) with stopping power routines by K. Lesko (1984)].
 - [18] T. J. Ross *et al.*, Phys. Rev. C **85**, 051304(R) (2012).
 - [19] J. M. Allmond - Unpublished data.
 - [20] J. M. Allmond *et al.*, Phys. Rev. C **81**, 064316 (2010).
 - [21] J. Barrette, M. Barrette, S. Monaro, S. Santhanam, and S. Markiza, Canadian Journal of Physics **48**, 1161 (1970).
 - [22] L. V. Groshev, A. M. Demidov, V. A. Ivanov, V. N. Lutsenko, and V. I. Pelekhov, Nuclear Physics **43**, 669 (1963).
 - [23] F. Bečvář, R. E. Chrien, and O. A. Wasson, Nuclear Physics A **236**, 173 (1974).
 - [24] R. A. Kenefick and R. K. Sheline, Physical Review **133**, B25 (1964).
 - [25] E. R. Reddingius and H. Postma, Nuclear Physics A **137**, 389 (1969).
 - [26] J. Konijn *et al.*, Nuclear Physics A **373**, 397 (1982).
 - [27] J. L. Wood - private communication.
 - [28] T. Takemasa, M. Sakagami, and M. Sano, Physics Letters **37**, 473 (1971).
 - [29] DWUCK4 - P.D. Kunz, University of Colorado (1974).
 - [30] N. Blasi *et al.*, Nuclear Physics A **624**, 433 (1997).
 - [31] H.-F. Wirth *et al.*, Physical Review C **69**, 044310 (2004).
 - [32] G. M. Crawley *et al.*, Physical Review C **23**, 589 (1981).
 - [33] G. M. Crawley, W. Benenson, D. Weber, and B. Zwieglinski, Phys. Rev. Lett. **39**, 1457 (1977).
 - [34] M. Nomura, Prog. Theor. Phys. **59**, 1771 (1978).
 - [35] G. M. Crawley, Proc. 1980 RCNP Int. Symp. on highly excited states in nuclear reactions, Osaka, 1980. ed. H Ikegami and M. Muraoka, 590.
 - [36] T. Nakagawa *et al.*, Nuclear Physics A **376**, 513 (1982).